MICHIGAN STATE UNIVERSITY

CYCLOTRON LABORATORY

FRAGMENTATION OF NUCLEAR SYSTEMS
A SIGNATURE FOR LIQUID-GAS PHASE INSTABILITIES

APOSTOLOS D. PANAGIOTOU

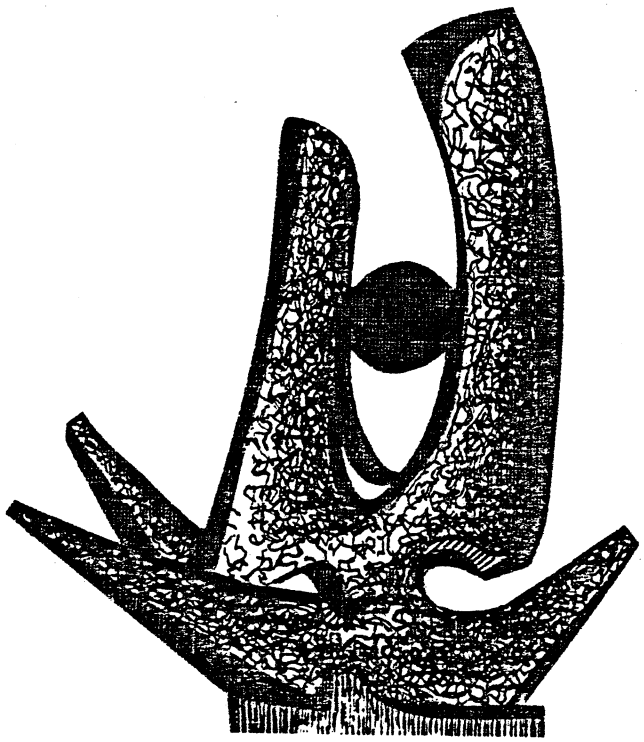

APRIL 1984

MSUCL-460

MSUCL-460
April 1984

FRAGMENTATION OF NUCLEAR SYSTEMS *

A SIGNATURE FOR LIQUID-GAS PHASE INSTABILITIES

APOSTOLOS D. PANAGIOTOU

National Superconducting Cyclotron Laboratory

Michigan State University, East Lansing, Michigan 48824 U.S.A.

and

Department of Physics, University of Athens
Nuclear Physics Laboratory, 104 Solonos Street
Athens 144, Hellas

ABSTRACT

The fragmentation of nuclear systems, created in proton and heavy ion induced reactions in a wide energy range, is examined. The dependence of the fragment production cross section on the incident energy and on the temperature of the emitting system is compared to predictions of a theory of condensation. Several instances are indicated where the fragmentation instability can be explained by and may be attributed to a Liquid-Gas phase transition. Several theoretical treatments are discussed. Conventional nuclear effects cannot fully describe the observed phenomena.

Invited talk to be presented at COLLOQUE GANIL, Giens, France, May 20-25, 1984

1. INTRODUCTION

Through the use of high energy nuclear collisions, it may become possible to create new forms of nuclear matter and to determine the nuclear equation of state. At these energies novel phenomena of the transient highly excited nuclear system may occur, manifesting themselves through multi-fragmentation and pion production processes. Although most attention has been directed towards such phenomena as phase transitions to a pion condensate or a quark-gluon plasma, conjectured to develop at high density and temperature, it is also possible that a Liquid-Gas phase instability may set in at a much lower critical temperature and density. This instability may be encountered during the expansion of the initially heated participant zone, formed in an energetic nuclear collision and manifest itself through the emission of complex nuclear fragments. Fig. 1 shows the hydrodynamiclal picture of a heavy ion collision and the expanding participant zone.

Possible experimental evidence and supporting theoretical treatments of critical phenomena, which (give credit to) the notion of a Liquid-Gas (L-G) phase transition in the expanding hot nuclear system, are presented. It is also shown that "conventional" phenomena, such as Coulomb barrier effects, cannot fully account for the observed behavior of the fragment distributions.

2. THEORETICAL CONSIDERATIONS

2-a. Equation of State

The properties of nuclear matter at finite temperatures and densities below normal (ρ_o=0.17 fm^{-3}) have been studied extensively (1-4 and references therein). It has been shown that in the Hartree-Fock approximation the nuclear matter exhibits the same properties as a van der Waals system (2). Calculations of the equation of state, assuming a uniform density and phenomenological or realistic interactions (5,3), have given isothermal pressure-versus-density curves similar to those of Figure 2. The magnitude of the critical quantities, ρ_c and T_c, for a Liquid-Gas phase transition vary in the range of 0.2-0.4 ρ_o and 8-20 MeV, respectively, depending on initial assumptions.

During the expansion and disassembly phase of the hot region along an isotherm, the nuclear density decreases until the freeze out density, ρ_f, is reached. At ρ_f collisions cease and the fragments move undisturbed, aside from final state interactions and internal deexcitation (6). To observe both liquid and gas phases at a certain temperature, the Maxwellian construction must encompass ρ_f. If ρ_f is large, the system will be mostly in the liquid phase at freeze out, whereas if ρ_f is very small, the system will have traversed the coexistence region and only the gas phase will exist. The quoted (7) value of ρ_f=0.4 ρ_o, approximately equal to the range of calculated ρ_c values, is comforting.

2-b. Theory of Condensation

Following the treatment of references (8-10) in the framework of a theory of condensation in excited nuclear matter, the probability for fragment formation of size A is given by :

$$P(A) \sim A^{-k} \exp\{[-a_s'(T)A^{2/3} - a_v'(T)A + \mu(T)A]/T\} \quad [1]$$

where k is the T-, A-independent critical exponent, $a_s'(T)$ is the surface free energy per particle, $a_v'(T)$ is the volume free energy per particle and $\mu(T)$ is the chemical potential per particle. With the following substitutions:

$$X = \exp[-a_s'(T)/T] \quad [2]$$

$$Y = \exp\{-[a_v'(T) - \mu(T)]/T\} \quad [3]$$

equation [1] assumes the following three forms, corresponding to the three regions L, L-G, G of Fig. 2 (see ref. 10):

$$P(A) \sim A^{-k} X^{A^{**}2/3}, \quad \text{for } T < T_c \quad [4]$$

$$P(A) \sim A^{-k}, \quad \text{for } T = T_c \quad [5]$$

$$P(A) \sim A^{-k} Y^A, \quad \text{for } T > T_c \quad [6]$$

It is noted that X and Y are less than 1.0 for all $T \neq T_c$ and that the pure power law dependence of the fragment distributions at $T = T_c$ is modulated by the exponential factors X and Y at temperatures $T<T_c$ and $T>T_c$, respectively.

Figure 3 shows indicatively the expected dependence of the fragment distributions on the temperature of the emitting system for three temperatures : $T < T_c$, $T = T_c$ and $T > T_c$. The curves

were calculated using the parameterization of ref. 10 for equations [4,6] above and assuming k = 2.0 and T_C = 12.0 MeV. The strong dependence of the slope on the temperature is evident.

3.ANALYSIS OF FRAGMENT DISTRIBUTIONS

3-a. Power Law Fits

To elucidate the temperature dependence of the fragment production cross section, the fragment distributions from proton and heavy ion induced reactions were fitted with a power law dependence of the form:

$$P(A) \sim A^{-\tau} \qquad [7]$$

where τ is the "apparent" exponent. In this approximation, the effects on the probability for fragment emission of the temperature-dependent factors X and Y, at $T < T_C$ and $T > T_C$, respectively, are absorbed into the power exponent. Therefore, the apparent exponent will vary with temperature and will reach a minimum value, that of the critical exponent k, at the critical temperature T_C.

The fragment distributions begin with $Z \geq 5$ or $A \geq 11$, since the liquid-drop expansion is valid only for large enough droplets. The temperatures were obtained from fragment energy distributions or from ideal Fermi-gas calculations (10). Fig. 4 shows the quality of typical least-squares fits to the fragment mass distributions for several systems and energies. The approximate power law dependence is evident. In Fig. 5 a dramatic temperature dependence of the apparent exponent is observed; τ decreases as the temperature increases up to

about 11-12 MeV, after which the trend is reversed. The exponent appears to reach a minimum value of less than 2.0 -a theoretically minimum vulue- in the temperature range of about 11-12 MeV. If the critical temperature, T_C, is assigned to the temperature corresponding to the minimum value of the apparent exponent, viz. corresponding to the maximum probability for fragment emission, then from Fig. 5 it may be infered that $T_C \sim$ 11-12 MeV. This value is in disagreement with recent estimates of the critical temperature of ~3.3 MeV, from fitting the isotope distributions in the p + Kr,Xe rections, although the temperature extracted from the fragment energy distributions was about 15 MeV (11,12).

A possible explanation of this discrepancy is that no account was taken of the particle-decay of the abundant excited neutron-rich (-deficient) isotopes. Not only the isotopes, produced in excited states above the very low neutron(proton) emission threshold (Bn(p) > ~ 0.3 MeV) will decay, but also a portion of those originally produced in the ground state, due to the continuous nucleon-fragment interaction (inelastic excitation) in the expanding system (13). This interaction may result in substantial "cooling" of the system (14). Therefore, the detected isotope yield may by far not reflect the yield produced in the hot system and consequently the system's temperature.

A recent treatment (15) of the expansion phase of a hot nuclear system, created in an energetic heavy ion collision, using a selfconsistent field-theoretical model which considers dynamical growth of instabilities, produces a sequence of the expansion and the corresponding fragment distributions for several temperatures shown in Fig. 6. Note in particular the quite flat distribution at T=15 MeV

compared to the strong fall off at T=50 MeV and to the minimal yield at T=8 MeV. The values of the temperature are only indicative and do not characterize critical and non-critical regions.

3-b. Cross Section Ratios

In Fig. 3 the slope of the distributions for both $T < T_C$ and $T > T_C$ is steeper than that for $T = T_C$, but should approach it as the temperatures approach T_C. As a consequence, the ratio of the cross section : $R = \sigma(A_1)/\sigma(A_2)$, of any two masses of the distribution, where $A_1<A_2$, should increase as the temperature moves away from T_C, since $\sigma(A_2)$ decreases faster than $\sigma(A_1)$ with temperature.

This change of the slope of the fragment distributions with temperature should manifest itself also as a function of incident energy. Fig. 7 shows the dependence of the ratio of the fragment cross sections for Z = 6 and Z = 12 on the incident energy, for the systems C + Au and Ne + Au, in the energy range of 15 to 84 MeV/A and 250 to 2100 MeV/A, respectively (16-18).

The ratio decreases as the incident energy increases up to about 50 to 60 MeV/A and then the trend is reversed at higher energies. A likely interpretation of this behavior is that for C + Au, the fragment emitting system reaches the critical temperature at some incident energy between 30 and 84 MeV/A, corresponding to the minimun value of the ratio, viz. to the flatest slope. The indication from Ne + Au is that, as the temperature further increases with energy, the ratio increases as well.

Proton induced fragmentation exhibits a somewhat different behavior, in that limiting energy deposition on the target by the proton beam sets in at high energies. This is reflected in the saturation of the fragment production cross section, which sets in at about 5 GeV, as shown in Fig. 8 for the radionuclides 18F and 24Na. Correspondingly, a limiting temperature in the fragment- emitting system should also be expect. This is shown in Fig. 9, where the temperature, calculated by moving source fits to the fragment distributions, is plotted as a function of the incident energy. Since the temperature of the system reaches a limiting value for energies higher than a few tens of GeV, the slope of the fragment distributions should also reach a limit at these energies.

This is shown in Fig. 10, where the ratio of the total cross section for the nuclides 18F and 24Na, produced in proton induced reactions on Ag, Kr and Xe in the incident energy range between 0.48 and 350 GeV is plotted (19,20,11). This ratio reaches a minimum value at an incident energy of the order of 5 GeV and then increases to a limiting value at very high energies. The minimum at about 5 GeV may indicate that the system has reached the critical temperature near this incident energy.

The dependence of the apparent exponent, τ, on the incident energy for the systems p + Ag in the energy range of 0.21 to 4.9 GeV (19,21,22) and in p + Kr, Xe in the energy range of 80 to 350 GeV, is shown in Fig. 11. t decreases with increasing energy up to about 5 GeV and then the trend is reversed, leveling off at very high energies. As in Fig. 10, there is an indication for a departure from a smooth and asymptotic behavior. It has been suggested that Coulomb

barrier effects between the source and the emitted fragments may account for a smooth dependence of the fragment yield on the temperature (23,24).

An estimate of the decrease in the fragment production cross section due to the Coulomb barrier penetration can be obtained from the penetrability factor:

$$P(A) \sim \exp\{-2\int^{R_f} [\, 2m/h^2\, (\, V(x) - E\,)]^{1/2}\, dx\,\} \qquad [9]$$

where R_f is R(V=E), m is the nucleon mass, V is the Coulomb barrier seen by each fragment and E is the distribution of the fragment kinetic energy before emission at each temperature. This factor is multiplied by the fragment yield at the high energy region ($Y(A) \sim A^{-3.0}$). The resulting mass distributions for $11 \lesssim A \lesssim 25$, fitted by a power law of the form:

$$A^{-\tau} \sim P(A)\, A^{-3.0} \qquad [10]$$

are also shown in Fig. 11, normalized to the 0.21 GeV point. The spread of the curves reflects the assumed ±1 MeV uncertainty in the temperature of the source at each energy. The smooth and asymptotic dependence of the apparent exponent, incurred when Coulomb effects are incorporated, is evident. The departure from the smooth shape -a smooth curve joining the 0.48 and 80 GeV points- which is at least 2 standard deviations at the 4.9 GeV point, may indicate the occurence of "non-conventional" fragmentation phenomena.

4. CALCULATIONS OF CRITICAL QUANTITIES

Recent calculations for finite nuclear systems (25), using a Skyrme effective interaction and finite temperature Hartree-Fock theory, predict the critical temperature to be in the range of 9.5 to 13.5 MeV. Also Hartree-Fock calculations at finite temperature, which include the contribution of unbound states and use Skyrme SIII and SKM interactions, predict critical temperatures of the order of 11 and 8 MeV, respectively (1). Evaluation of thermal properties of finite nuclei (26), using the thermal Hartree-Fock approximation and the Skyrme III interaction, yield a critical temperature T_c=11.82 MeV for the liquid drop surface tension. Extended Fermi-gas model calculations (27), in which the potential energy is treated within Bruekner's energy-density formalism and appropriate corrections due to surface and asymmetry effects were included, predict a diminishing surface tension at a critical temperature of approximately 11 to 13 MeV, for a nuclear compressibility constant K in the range of 180 to 250 MeV, Fig. 12. Finally, a semiclassical treatment of hot semi-infinite nuclear matter (4), using a realistic Skyrme force, predicts a vanishing surface free energy at the critical temperature of 14.6 MeV and critical density of $0.33\rho_o$. All of the above theoretical predictions are in good agreement with the estimation of the critical temperature from the analysis of the fragment distributions presented.

V. SUMMARY AND CONCLUSIONS

In this paper it is suggested that fragmentation instabilities in hot nuclear systems may be viewed as signatures for Liquid-Gas phase transitions. A theory of condensation, used to analyze and interpret the fragmentation systematics, has been successful in accounting for most of the features of the data. The critical temperature in the region of 11 to 12 MeV for a phase transition, obtained from the analysis of the complex fragment distributions in proton and heavy ion induced reactions, is well within several theoretical calculations.

In this treatment, the formation of thermalized matter of nuclear dimensions is assumed. Calculations of the time scale for such thermalization indicate that it is possible at the later expansion stage of the system and for temperatures greater than about 7-8 MeV (28-31). It is interesting that this time-constrained lower limit for the temperature of the system is substantially lower than the estimated critical temperature of 11-12 MeV. Since a L-G phase instability exists only for temperatures below the critical temperature and above the minimum temperature for phase equilibration, it is clear that if the latter temperature were higher than the former, the L-G instability would not develop. Furthermore, the close proximity of the freeze out density to the critical density, $\rho_f \sim \rho_c \sim 0.4\ \rho_o$, is encouraging.

Both of the above concepts are generally accepted at high energies; there is, however, conflicting evidence whether equilibration is fully accomplished in the intermediate energy regime. Clearly, systematic and detailed fragmentation data from proton and

heavy ion induced reactions are needed to determine accurately the critical quantities and eventually the equation of state for the hot nuclear system. This information will also provide insight into the hydrodynamical behavior, necessary for the occurrence of more exotic phase transitions, and for the astrophysical ramifications with regard to neutron stars and supernovae (8,30).

ACKNOWLEDGEMENTS

I am grateful to many colleques for discussions, ideas and unpublished data pertaining to this paper. In particular I would like to thank D.H. Boal, M.W. Curtin, R.E.L. Green, D.K. Scott, P.J. Siemens, H. Toki and G.D. Westfall. I also wish to thank the NSCL at Michigan State University for their hospitality while this work was carried out.

* Work supported by NSF Grant No. PHY-83-12245

REFERENCES

1. P. Bonche, S. Levit and D. Vautherin, Preprint S.Ph.T/83/85
2. U.Mosel, P.G.Zint, K.H.Passler, Nucl. Phys. A236, 252 (1974)
3. B. Friedman, V.R.Pandharipande, Nucl. Phys. A361, 502 (1981)
4. J. Bartel et al, Preprint TPR-83-21
5. P. Danielewicz, Nucl. Phys. A314, 465 (1979)
6. A.Z. Mekjian and D.S. Gupta, Phys. Rep. 72C, 133 (1981)
7. M-C. Lemaire et al, Phys. Lett. 85B, 38 (1979)
8. P.J. Siemens, Nature Vol. 305, 410 (1983) and ref's therein
9. M.E. Fisher, Physics 3, 255 (1967)
10. A.D. Panagiotou, M.W. Curtin, H. Toki, D.K. Scott and P.J. Siemens, Phys. Rev. Lett. 52, 496 (1984) and to be published.
11. A. S. Hirsch et al, Phys. Rev. C29, 508 (1984)
12. R.W. Minich et al, Phys. Lett. 118B, 458 (1982)
13. D. H. Boal MSUCL- 458 ,1984
14. D.J. Morrissey et al, MSUCL- 454, 1984
15. B. Strack and J. Knoll, Z. Phys. A315, 249 (1984)
16. C.B. Chitwood et al, Phys. Lett. 131B, 289 (1983)
17. U. Lynen et al, Nucl. Phys. A387, 129c (1982)
18. A.I. Warwick, et al, Phys. Rev. C27, 1083 (9183)
19. R.E.L.Green, R.G.Korteling and K.P.Jackson, TRI-PP-83-118Report
20. A.A.Caretto, J.Hudis, G.Friedlander, Phys. Rev. 110, 1130 (1958)
21. R.E.L. Green, R.G. Korteling, Phys. Rev. C22, 1594 (1980)
22. G.D. Westfall et al, Phys. Rev. C17, 1368 (1978)
23. D.H.E. Gross et al, Z. Phys. A309, 41 (1982)
24. D.H. Boal, Preprint MSUCL - 451, 1984
25. H.Jaqaman, A.Z.Mekjian, L.Zamick, Phys. Rev. C27, 1782(1983)

26. G.Sauer, H.Chandra and U.Mosel, Nucl. Phys. A264, 221 (1976)
7. W. Stocker and J. Burzlaff, Nucl. Phys. A202, 265 (1973)
28. D.H. Boal, Phy. Rev. C28, 2568 (1983)
29. M.W. Curtin, H. Toki, D.K. Scott, Preprint MSUCL- 426
30. D. K. Scott, MSUCL- 434, 1983
31. J. Cugnon, Phys. Lett. 135B, 374 (1984)

FIGURE CAPTIONS

FIG. 1. The participant-spectator picture of high energy heavy ion collision, calculated with a hydrodynamical model.

FIG. 2. Pressure versus density for nuclear matter. The three regions Liquid, L-G Coexistance and Gas are indicated (see also discussion in the text).

FIG. 3. Fragment distributions plotted on a relative scale for three temperatures of the emitting system. A critical exponent k=2.0 and a critical temperature T_c=12 MeV was assumed.

FIG. 4. Typical power law least-squares fits to the fragment mass distributions.

FIG. 5. The apparent exponent, τ, of the power law fit to the fragment distributions as a function of the temperature, T. The systems are: CIR- p+Ag, X- p+U, SQR- p+Xe and p+Kr, UTRI- C+Ag, DTRI- C+Au.

FIG. 6. The sequence of the expansion and the corresponding fragment distributions for several temperatures of a hot nuclear system formed in a heavy ion collision.

FIG. 7. The ratio of the cross section for Z=6 to Z=12 as a function of the incident energy per nucleon. The 15 MeV/A and 250 MeV/A points are normalized to 1.0

FIG. 8. Excitation function for the yield of the nuclides 18F and 24Na in proton induced reactions on Ag.

FIG. 9. The temperature of fragment-emitting system versus the proton incident energy. The temperatures are obtained from moving source fits to the fragment energy distributions.

FIG. 10. The ratio of the total cross section of 18F to 24Na as a function of the incident proton energy. The 0.48 GeV point is normalized to 1.0

FIG. 11. The apparent exponent, τ, as a function of the incident energy for the systems p + Ag and p + Kr,Xe. The curves depict the dependence of the calculated apparent exponent on the Coulomb barrier effects (see discussion in the text).

FIG. 12. The dependence of the surface tension on the temperature for several values of the compressibility constant K.

MSUX-81-328

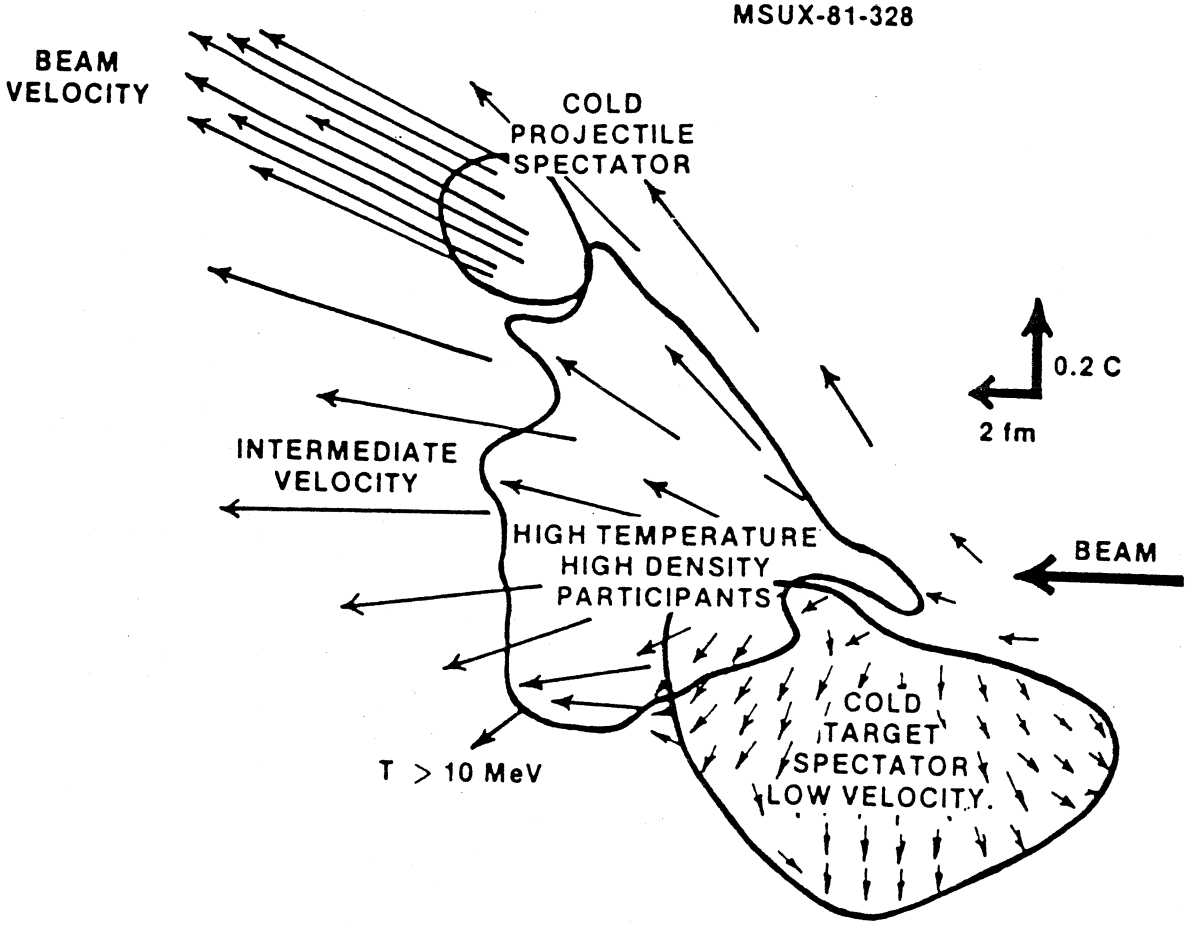

^{20}Ne on U. at 400 MeV/NUCLEON
TEMPERATURE, DENSITY & VELOCITY PROFILES.
IN HYDRODYNAMICS
FAST TIME EVOLUTION
MEAN FREE PATH ⟶ 0

Fig 1.

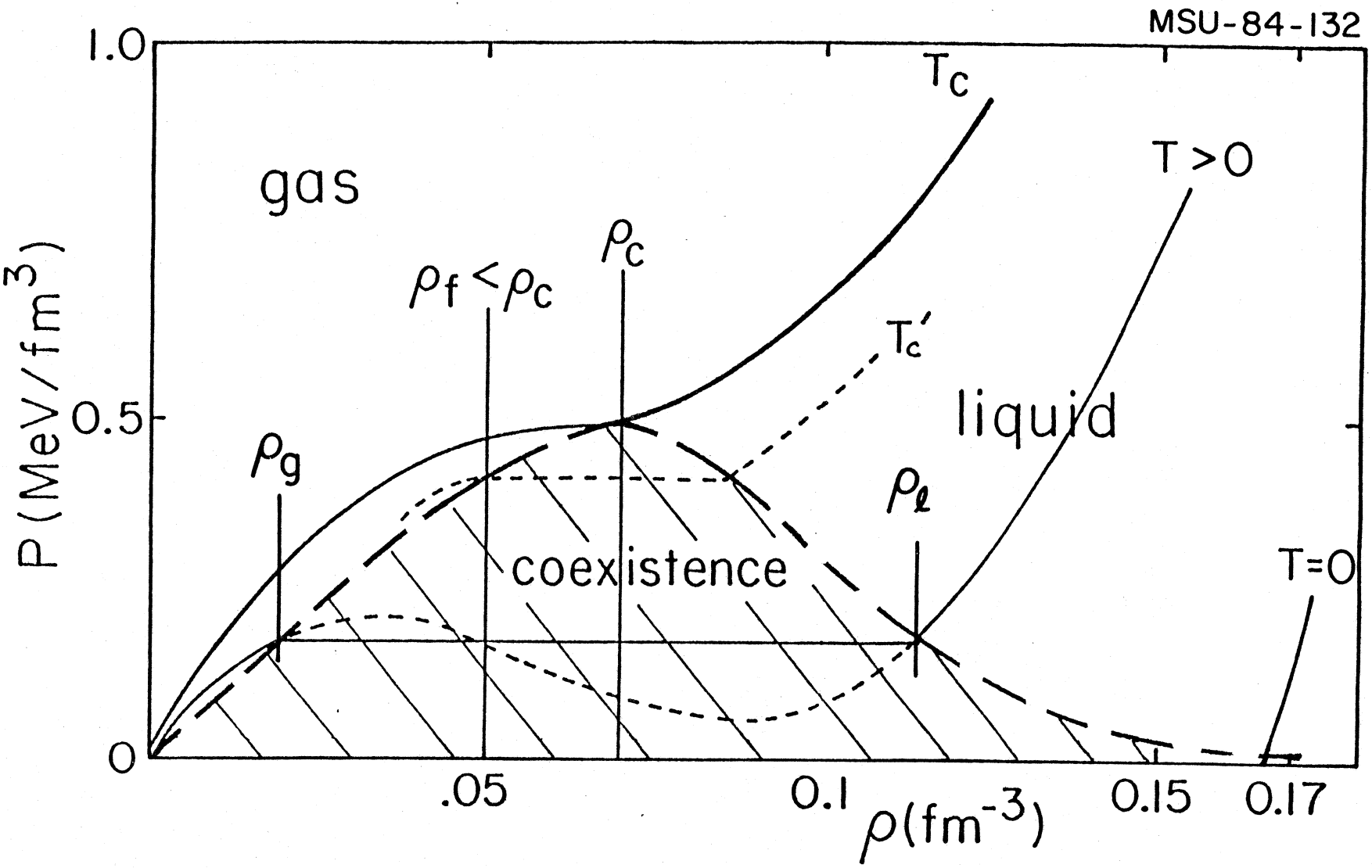
MSU-84-132
1.0
0.5
0
P (MeV/fm^3)
T_c
T>0
gas
$\rho_f < \rho_c$
ρ_c
T_c'
liquid
ρ_g
ρ_l
coexistence
T=0
.05
0.1
ρ(fm^{-3})
0.15
0.17

Fig. 2

MSU-84-129

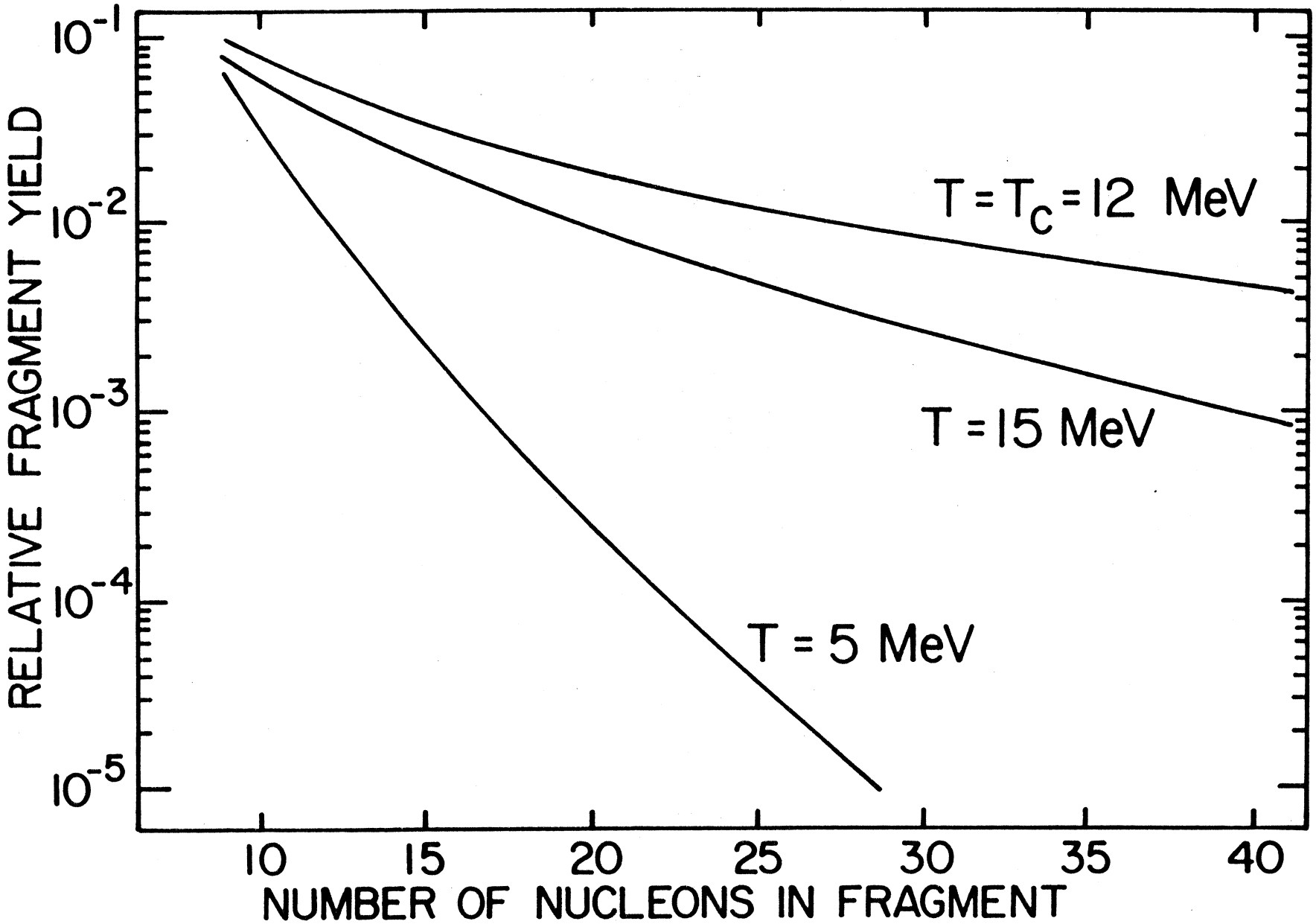

Fig. 3

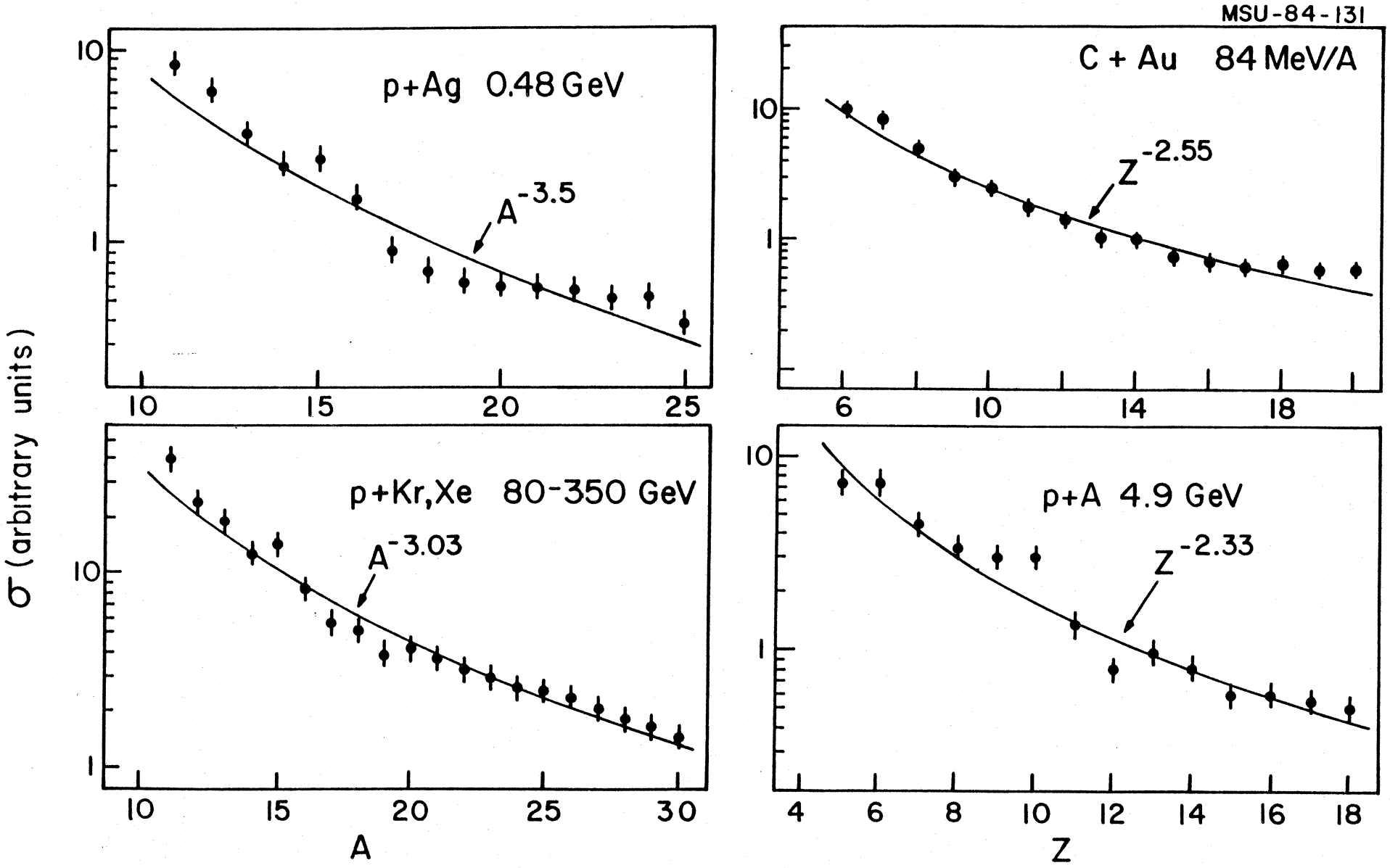
p+Ag 0.48 GeV
A^-3.5
C + Au 84 MeV/A
Z^-2.55
p+Kr,Xe 80-350 GeV
A^-3.03
p+A 4.9 GeV
Z^-2.33
σ (arbitrary units)
A
Z

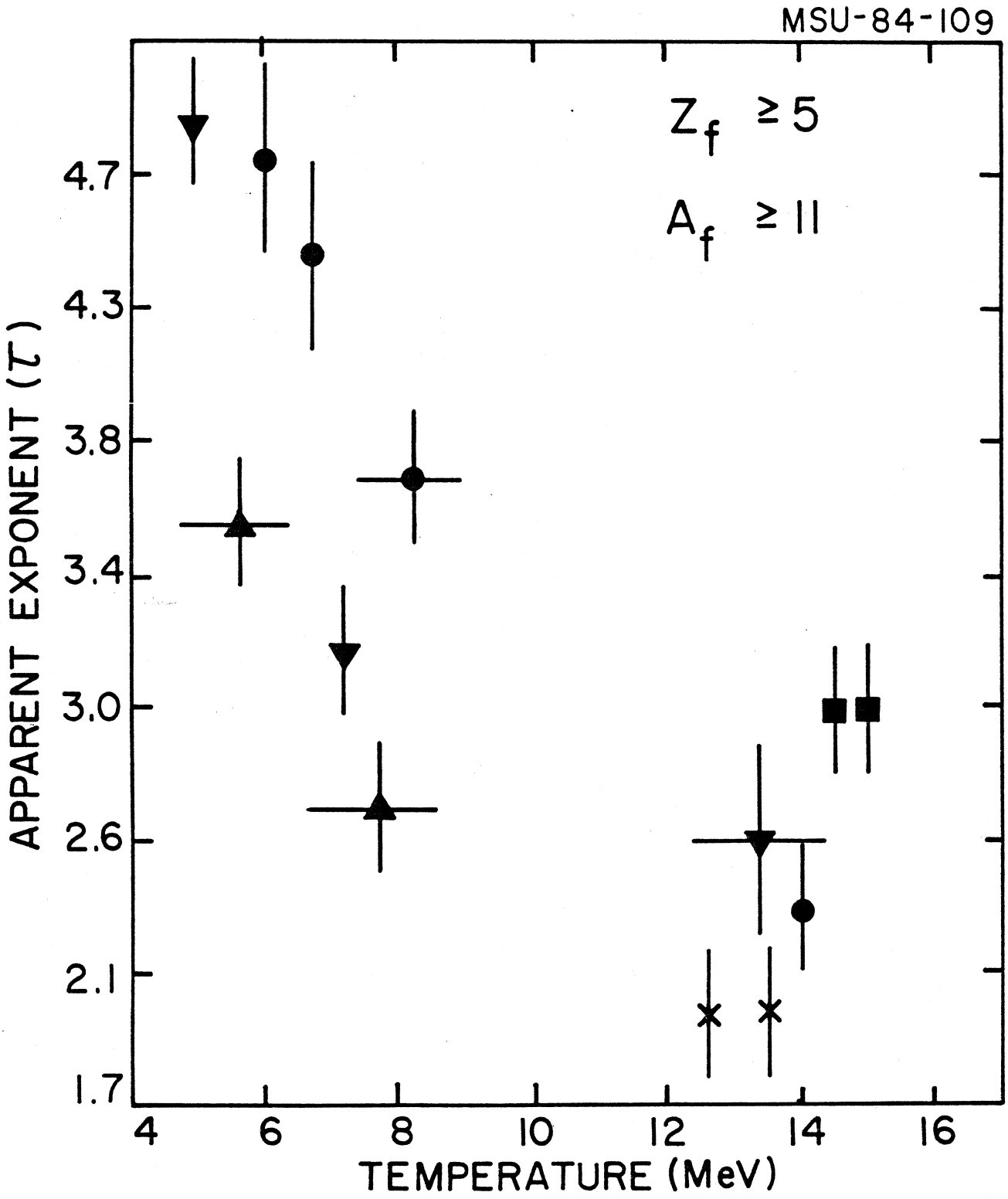
MSU-84-109
$Z_f \geq 5$
$A_f \geq 11$
APPARENT EXPONENT (τ)
4.7
4.3
3.8
3.4
3.0
2.6
2.1
1.7
4
6
8
10
12
14
16
TEMPERATURE (MeV)

Fig. 5

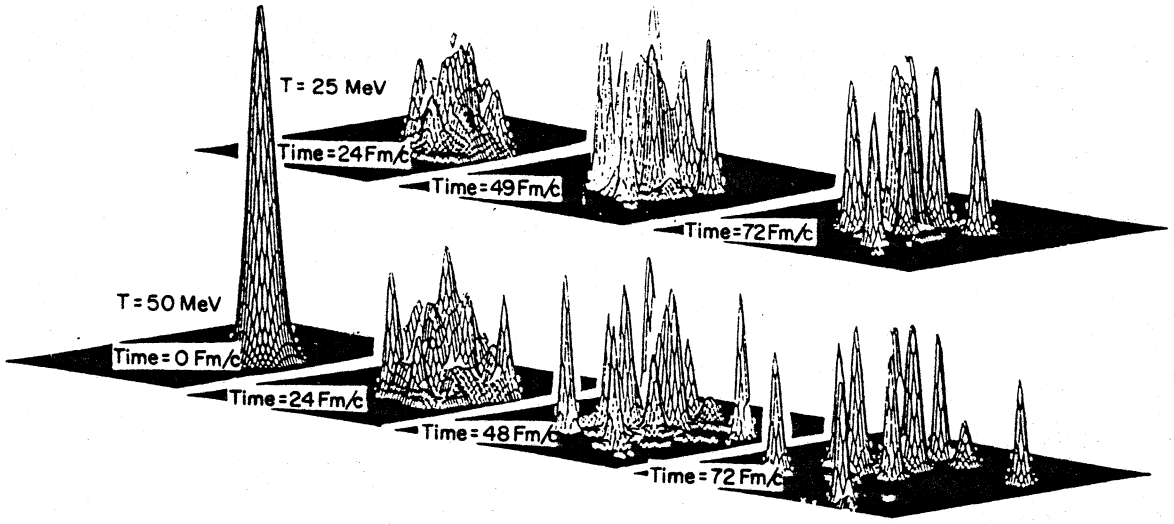
T = 25 MeV
Time = 24 Fm/c
Time = 49 Fm/c
Time = 72 Fm/c
T = 50 MeV
Time = 0 Fm/c
Time = 24 Fm/c
Time = 48 Fm/c
Time = 72 Fm/c

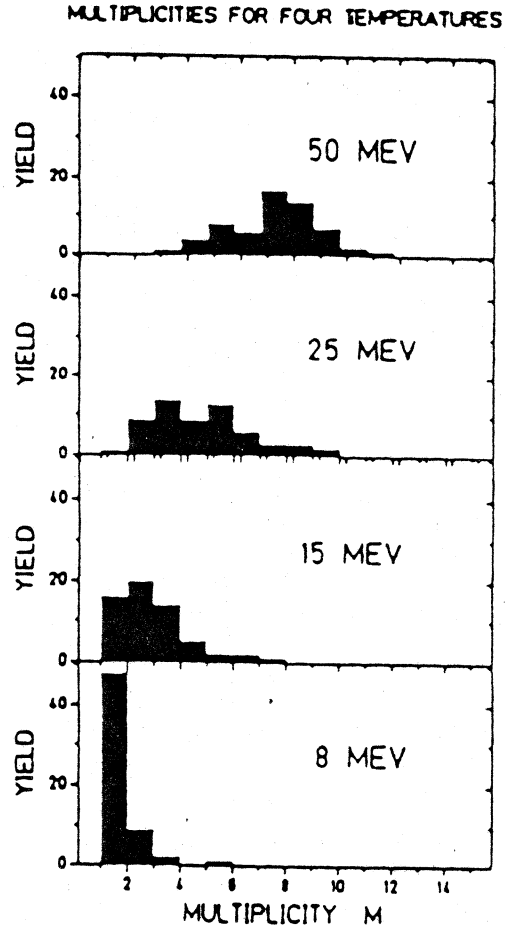
MULTIPLICITIES FOR FOUR TEMPERATURES
YIELD
50 MEV
25 MEV
15 MEV
8 MEV
MULTIPLICITY M

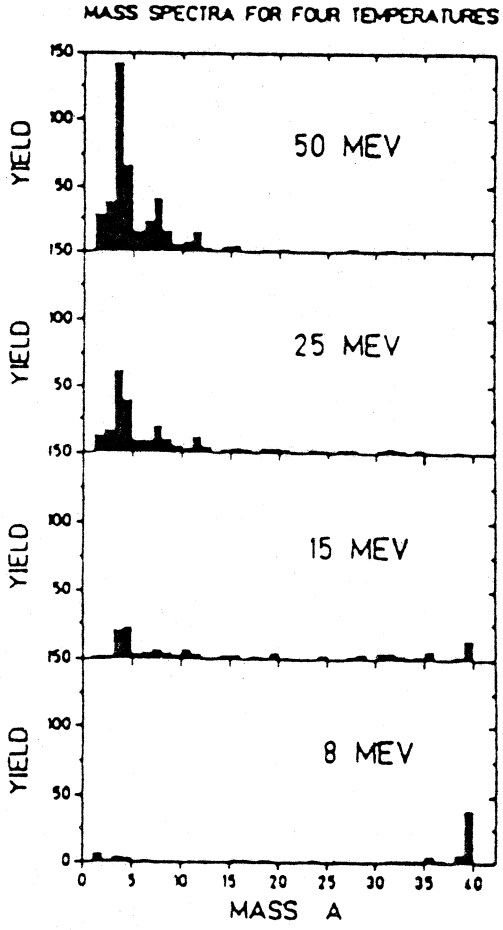
MASS SPECTRA FOR FOUR TEMPERATURES
YIELD
50 MEV
25 MEV
15 MEV
8 MEV
MASS A

Fig. 6

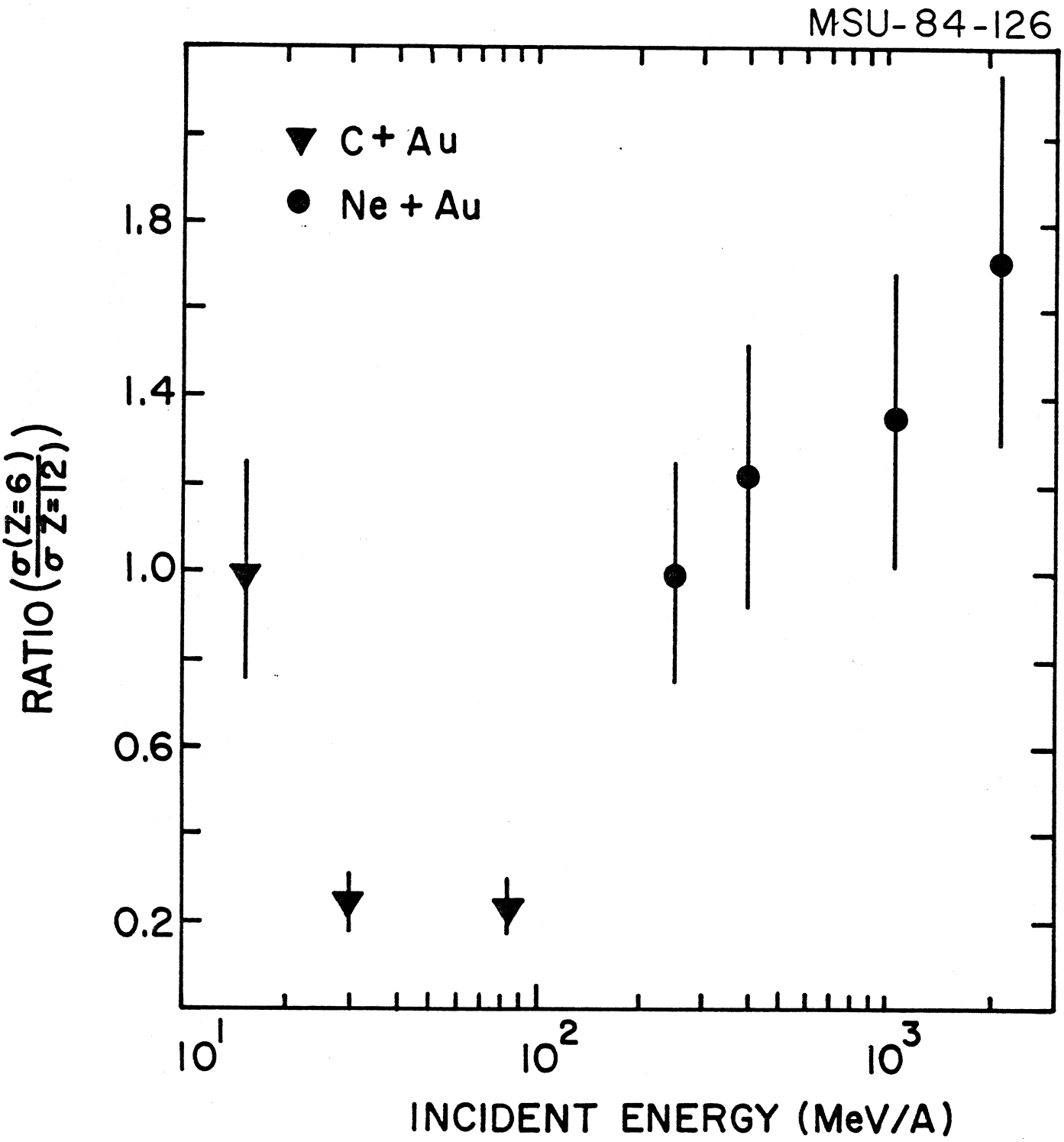
MSU-84-126
C + Au
Ne + Au
1.8
1.4
1.0
0.6
0.2
RATIO $(\frac{\sigma(Z=6)}{\sigma(Z=12)})$
10^1
10^2
10^3
INCIDENT ENERGY (MeV/A)

Fig. 7

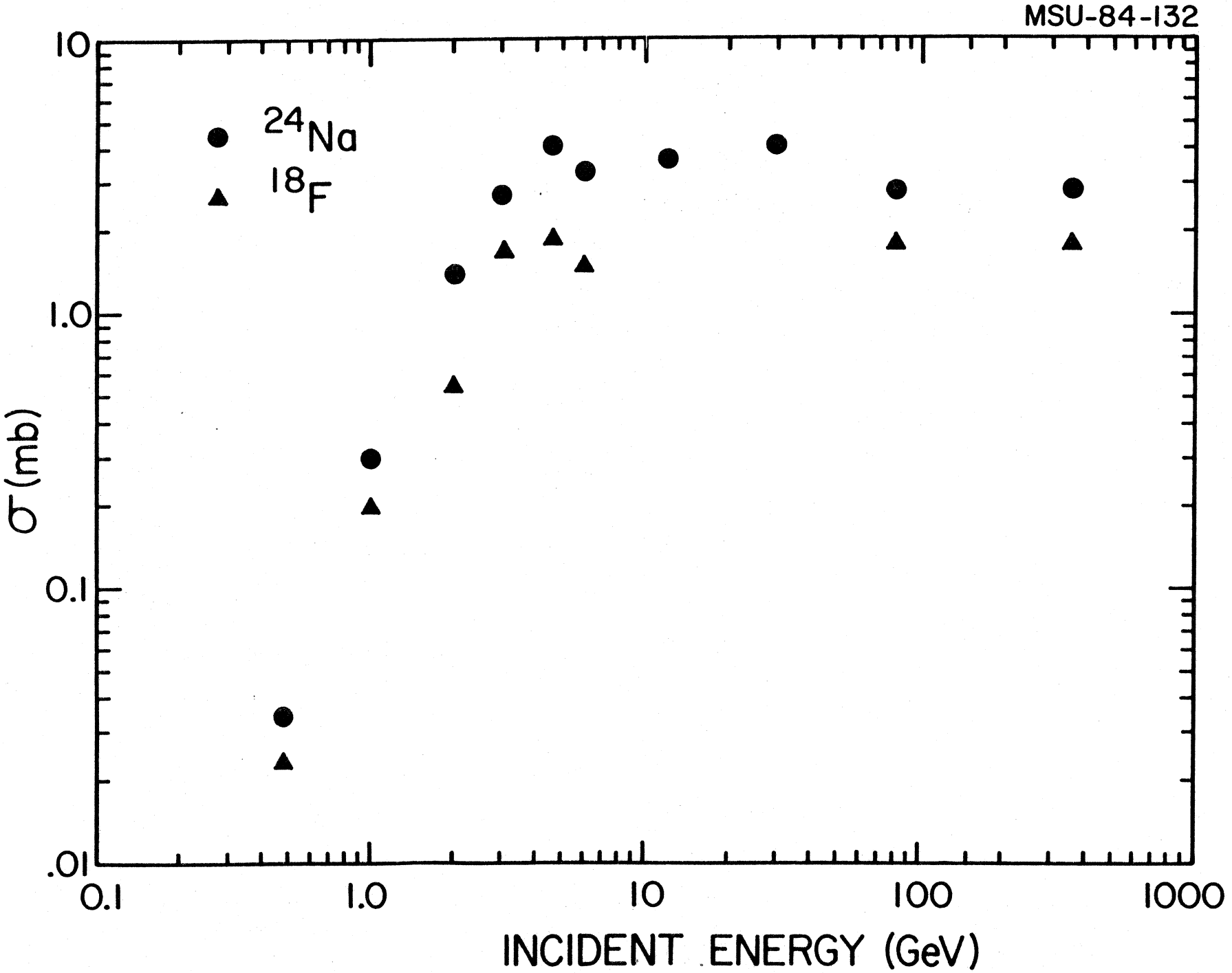
MSU-84-132
10
1.0
.1
.01
σ (mb)
^{24}Na
^{18}F
0.1
1.0
10
100
1000
INCIDENT ENERGY (GeV)

Fig. 8

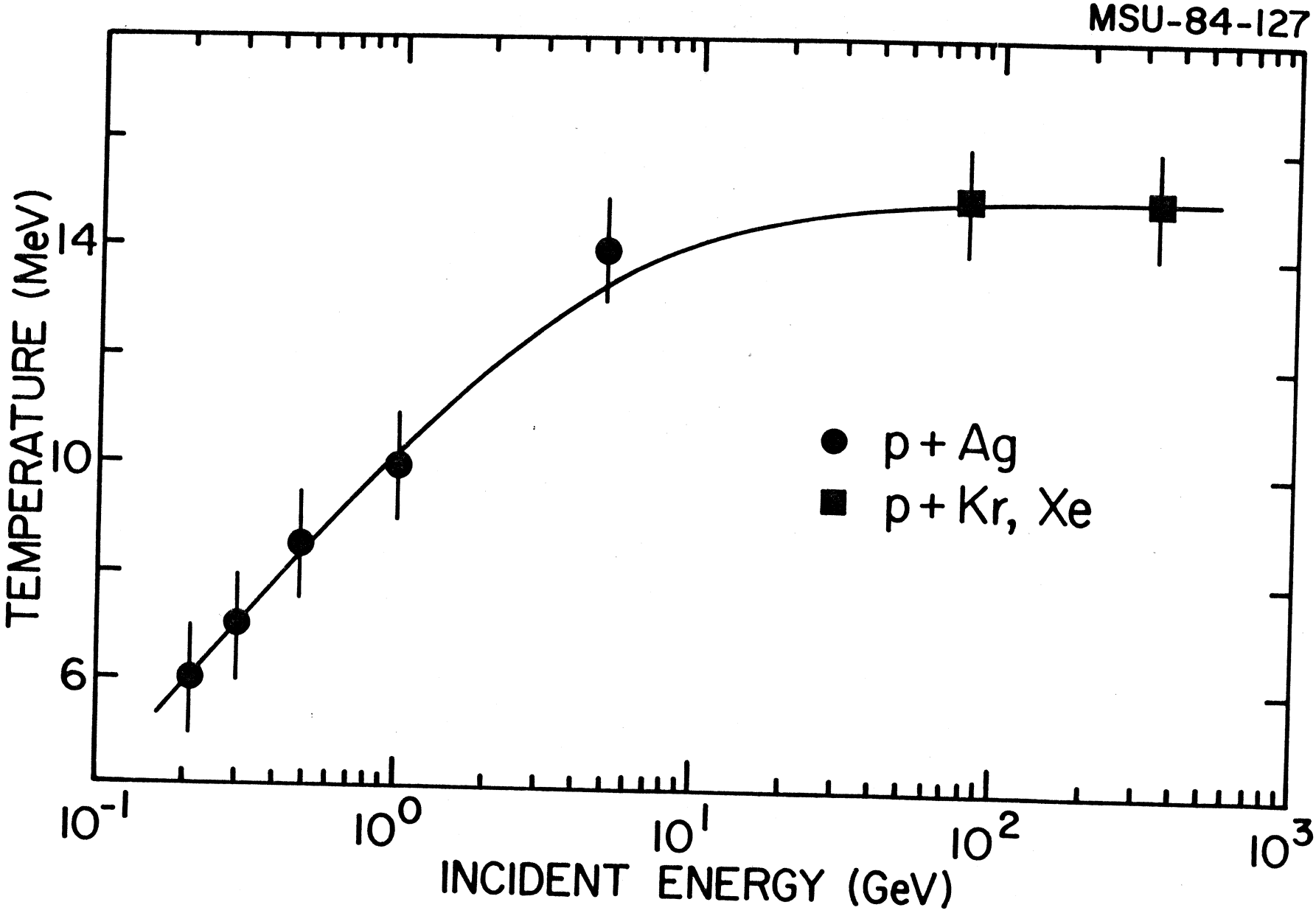
MSU-84-127
TEMPERATURE (MeV)
14
10
6
10^{-1}
10^{0}
10^{1}
10^{2}
10^{3}
INCIDENT ENERGY (GeV)
p + Ag
p + Kr, Xe

Fig. 9

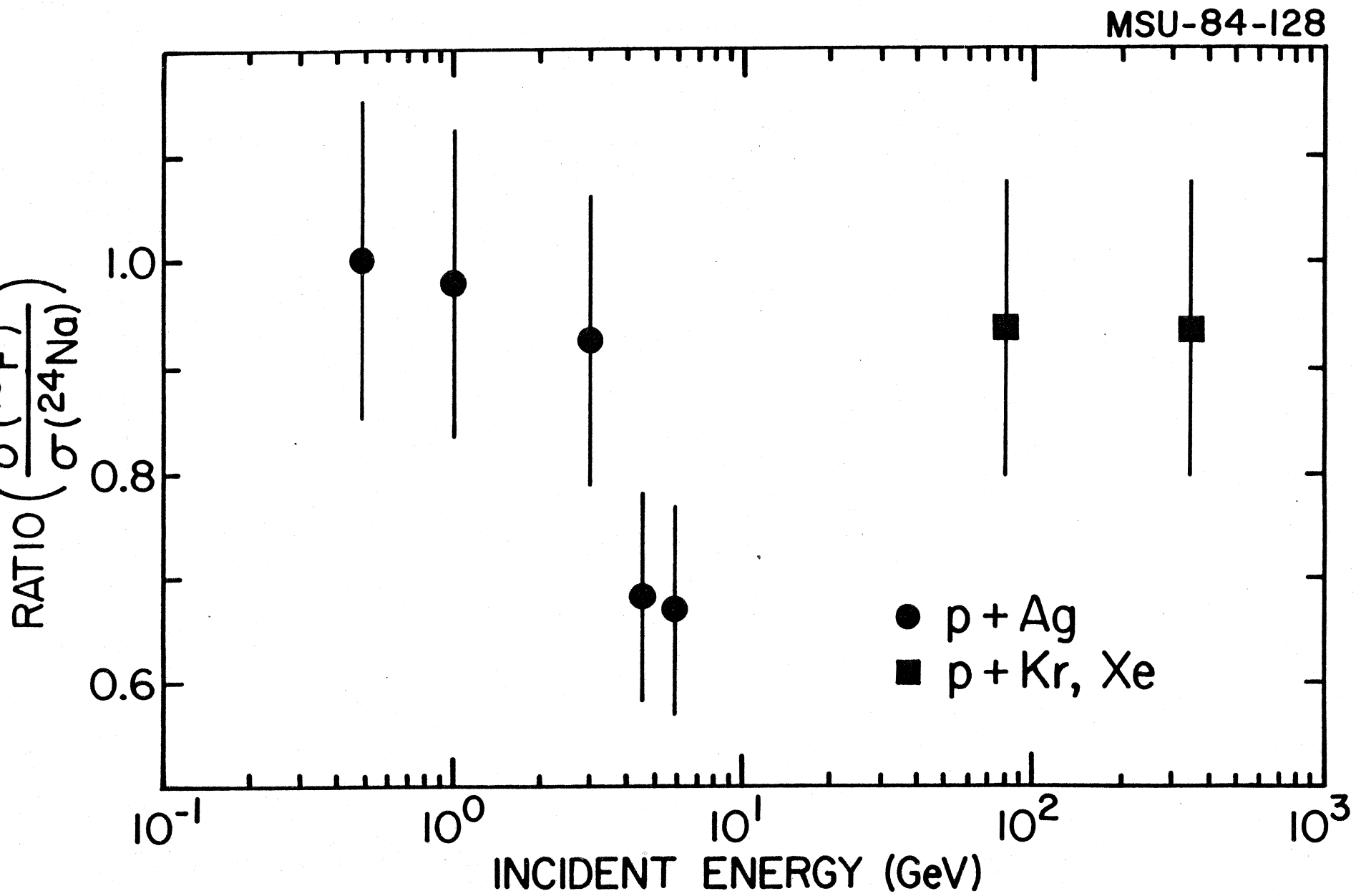
MSU-84-128
RATIO $\left(\frac{\sigma(^{18}F)}{\sigma(^{24}Na)}\right)$
1.0
0.8
0.6
10^{-1}
10^{0}
10^{1}
10^{2}
10^{3}
INCIDENT ENERGY (GeV)
p + Ag
p + Kr, Xe

Fig. 10

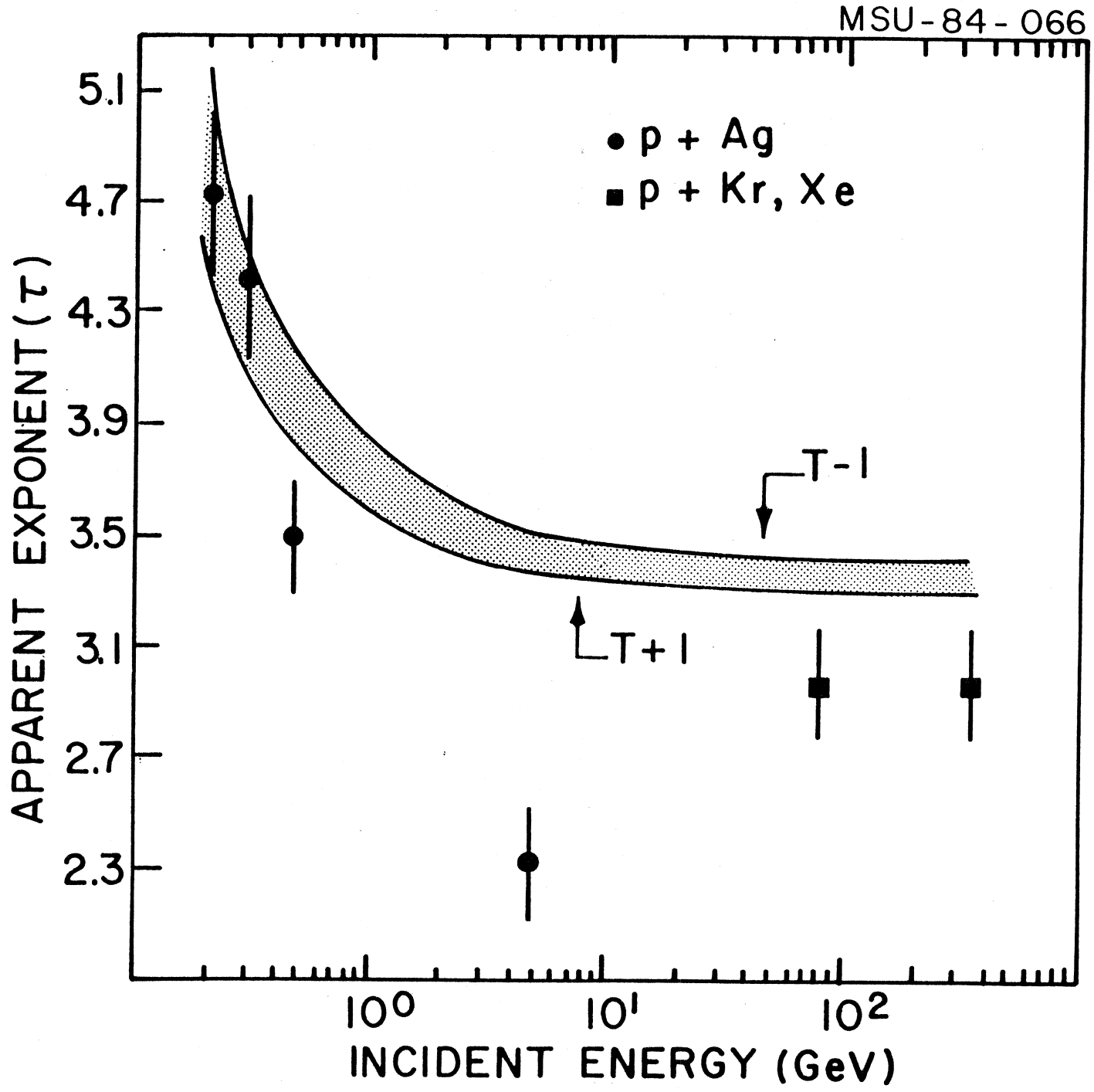
MSU-84-066
5.1
4.7
4.3
3.9
3.5
3.1
2.7
2.3
APPARENT EXPONENT (τ)
● p + Ag
■ p + Kr, Xe
T-1
T+1
10⁰
10¹
10²
INCIDENT ENERGY (GeV)

Fig. 11

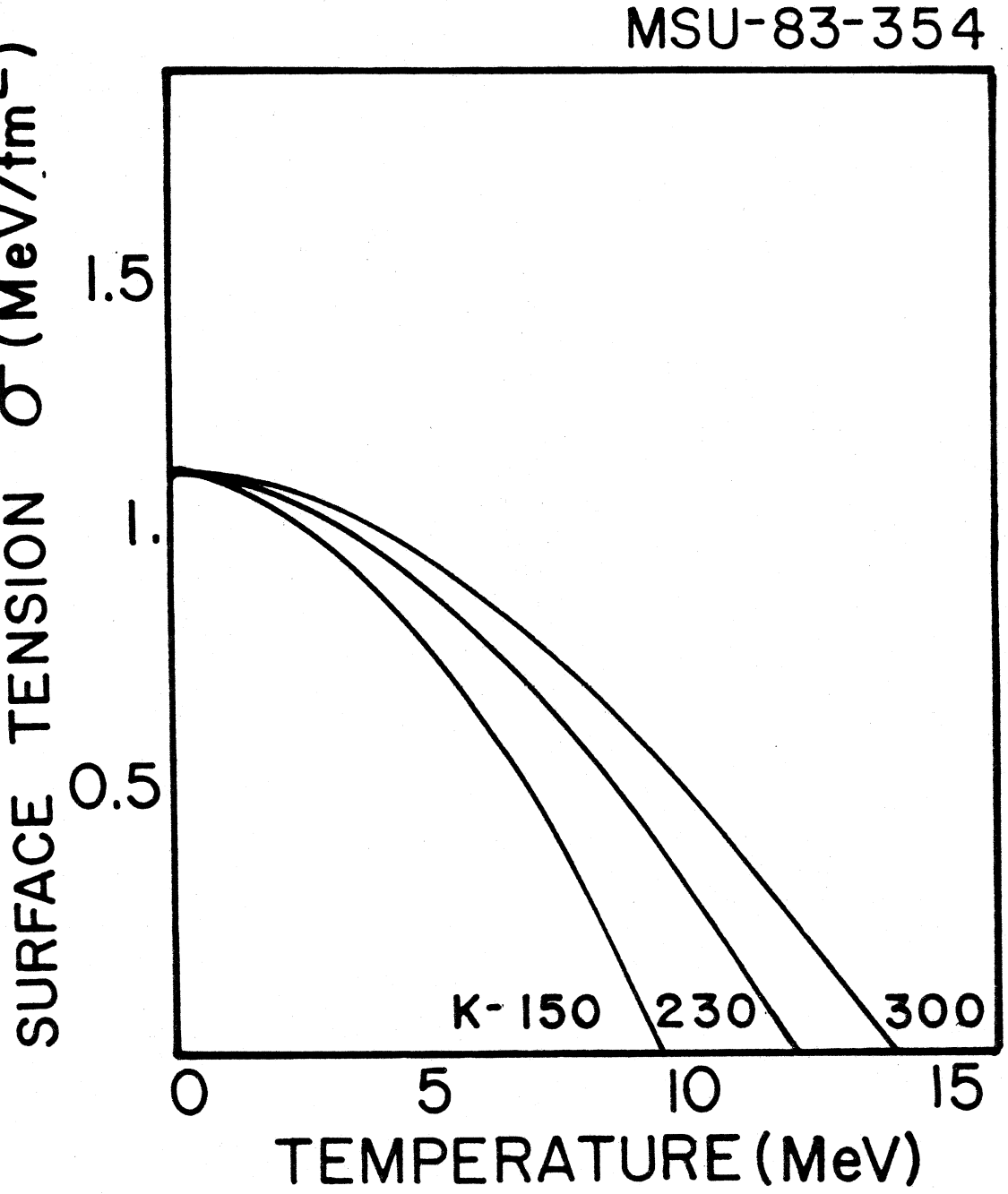
MSU-83-354
SURFACE TENSION σ (MeV/fm²)
1.5
1.
0.5
K-150
230
300
0
5
10
15
TEMPERATURE (MeV)

Fig. 12